Effect of sea-ice melt on inherent optical properties and vertical distribution of solar radiant heating in Arctic surface waters

Granskog, Mats A.; Pavlov, Alexey K.; Sagan, Sawomir; Kowalczuk, Piotr; Raczkowska, Anna; Stedmon, Colin

Published in:
Journal of Geophysical Research: Oceans

Link to article, DOI:
10.1002/2015jc011087

Publication date:
2015

Document Version
Publisher's PDF, also known as Version of record

AGU PUBLICATIONS

Journal of Geophysical Research: Oceans

RESEARCH ARTICLE
10.1002/2015JC011087

Special Section:
Forum for Arctic Modeling and Observational Synthesis (FAMOS): Results and Synthesis of Coordinated Experiments

Key Points:
- Sea-ice melt introduces a transparent surface layer
- Sea-ice melt dilutes CDOM absorption in Arctic surface waters
- Radiant heating shifts to deeper depths with sea-ice meltwater layers in late summer

Correspondence to:
M. A. Granskog,
mats.granskog@npolar.no

Citation:
Granskog, M. A., A. K. Pavlov, S. Sagan, P. Kowalczuk, A. Raczkowska, and C. A. Stedmon (2015), Effect of sea-ice melt on inherent optical properties and vertical distribution of solar radiant heating in Arctic surface waters, *J. Geophys. Res. Oceans*, *120*, 7028–7039, doi:10.1002/2015JC011087.

Received 30 JUN 2015
Accepted 30 SEP 2015
Accepted article online 5 OCT 2015
Published online 30 OCT 2015

Effect of sea-ice melt on inherent optical properties and vertical distribution of solar radiant heating in Arctic surface waters

Mats A. Granskog[1], Alexey K. Pavlov[1], Sławomir Sagan[2], Piotr Kowalczuk[2], Anna Raczkowska[2,3], and Colin A. Stedmon[4]

[1]Norwegian Polar Institute, Fram Centre, Tromsø, Norway, [2]Institute of Oceanology, Polish Academy of Sciences, Sopot, Poland, [3]Centre for Polar Studies, Leading National Research Centre, Sosnowiec, Poland, [4]National Institute of Aquatic Resources, Technical University of Denmark, Charlottenlund, Denmark

Abstract The inherent optical properties (IOPs) of Polar Waters (PW) exiting the Arctic Ocean in the East Greenland Current (EGC) and of the inflowing Atlantic waters (AW) in the West Spitsbergen Current (WSC) were studied in late summer when surface freshening due to sea-ice melt was widespread. The absorption and attenuation coefficients in PW were significantly higher than previous observations from the western Arctic. High concentrations of colored dissolved organic matter (CDOM) resulted in 50–60% more heat deposition in the upper meters relative to clearest natural waters. This demonstrates the influence of terrigenous organic material inputs on the optical properties of waters in the Eurasian basin. Sea-ice melt in CDOM-rich PW decreased CDOM absorption, but an increase in scattering nearly compensated for lower absorption, and total attenuation was nearly identical in the sea-ice meltwater layer. This suggests a source of scattering material associated with sea-ice melt, relative to the PW. In the AW, melting sea-ice forms a stratified surface layer with lower absorption and attenuation, than well-mixed AW waters in late summer. It is likely that phytoplankton in the surface layer influenced by sea-ice melt are nutrient limited. The presence of a more transparent surface layer changes the vertical radiant heat absorption profile to greater depths in late summer both in EGC and WSC waters, shifting accumulation of solar heat to greater depths and thus this heat is not directly available for ice melt during periods of stratification.

1. Introduction

The decrease of summer sea ice in the Arctic Ocean, of more than 10% in extent per decade since the 1980s, has numerous impacts on the functioning of the Arctic marine system, from the physics to ecology [*Meier et al*., 2014]. One important factor for the ecosystem is the change in the light availability in the ocean due to thinning of the ice pack [*Nicolaus et al*., 2012; *Hudson et al*., 2013] and even seasonal disappearance of the sea ice in large swaths of the Arctic Ocean formerly covered by a perennial ice cover [*Arrigo et al*., 2008]. From a biological perspective, elevated underwater light levels have been shown to result in increased Arctic Ocean primary productivity [*Arrigo et al*., 2008; *Popova et al*., 2012]. Also other photobiogeochemical processes are likely to be affected by the increased amount of solar light reaching the ocean, such as photobleaching of colored (or chromophoric) dissolved organic matter (CDOM), which in turn can affect both the underwater light field and photoproduction of labile substrates [*Bélanger et al*., 2006, 2013].

While we, in general terms, know that the amount of sunlight reaching the Arctic Ocean water column has increased [*Nicolaus et al*., 2012], the fate and factors controlling the penetration of light in the water column are not well described. Only a few studies have focused on documenting the factors controlling light penetration in the high-Arctic water column [*Pegau*, 2002; *Hill*, 2008; *Matsuoka et al*., 2011; *Bélanger et al*., 2013; *Pavlov et al*., 2015]. Generally, we know that CDOM plays an important role in light attenuation and surface heating in the Polar Waters of the Arctic Ocean and especially in adjacent shelf seas [*Pegau*, 2002; *Granskog et al*., 2007; *Hill*, 2008; *Pavlov et al*., 2015], and in the western Arctic, CDOM has been shown to contribute to 30–40% excess heating relative to pure seawater [*Pegau*, 2002; *Hill*, 2008]. The excess surface heating by CDOM is thus important for the melting of sea ice [*Hill*, 2008]. However, this likely varies regionally in the

Arctic Ocean, dependent on the distribution of terrigenous CDOM. Phytoplankton also play a role in light attenuation is surface Arctic waters but have a more transient nature [*Pegau*, 2002; *Pavlov et al*., 2015].

How the sea ice itself through melting contributes to the concentration and distribution of OAS (optically active substances) and thus inherent optical properties (IOPs) in the upper water column is less well known [cf. *Bélanger et al*., 2013]. The underwater light field is largely defined by the absorption and scattering by pure water and OAS (both organic and inorganic) in dissolved and particulate form in the water column [*Mobley*, 1994]. Main contributors to absorption are CDOM and particulates, the latter consisting largely of living organisms (phytoplankton) and detritus. Organic particulate material also contributes to light scattering along with a contribution from water molecules and inorganic particles [*Mobley*, 1994; *Kirk*, 1994]. Scattering essentially extends the path length of light in water within the same depth layer and hence increases net absorption per unit length. The combination and amount of OAS therefore play a critical role in spectral light penetration and heating rates in the surface ocean [*Pegau*, 2002; *Granskog et al*., 2007; *Hill*, 2008], with the latter potentially influencing primary production via enhanced stratification.

It has been shown that melting multiyear Arctic sea ice increases the scattering by particles in the surface waters in the Beaufort Sea (western Arctic), reducing levels of Photosynthetically Active Radiation (PAR, 400–700 nm), compared to an ambient homogeneous water column [*Bélanger et al*., 2013]. On the other hand, multiyear sea-ice melt did not provide excess CDOM to the water column [*Bélanger et al*., 2013; *Pegau*, 2002], contrary to what some previous studies have proposed [see *Scully and Miller*, 2000]. While a similar "dilution" effect of sea-ice melt on CDOM absorption was observed in western Fram Strait in the East Greenland Current (EGC), a region predominantly covered with younger ice [*Hansen et al*., 2013], no indication of increased particulates was observed [*Pavlov et al*., 2015] contrary to multiyear ice melting [cf. *Pegau*, 2002; *Bélanger et al*., 2013]. Thus, the impact of melting sea ice is likely dependent on the ambient water masses and the origin and type of sea ice that melts, which may vary seasonally and regionally. Since the Arctic ice pack has become younger [*Meier et al*., 2014] and regionally surface waters differ in their optical characteristics from those in the western Arctic [cf. *Stedmon et al*., 2011; *Pavlov et al*., 2015], there is a need to characterize the effect of sea ice melting on the optical properties also in other regions of the Arctic Ocean.

Here we report on the first high-resolution observations of IOPs in northern Fram Strait at a time of year when a significant freshening from sea-ice melt was apparent at the surface. The region also allows examining sea ice melting into optically contrasting water masses [see *Pavlov et al*., 2015], namely CDOM-rich and low-chlorophyll Polar Water from the Transpolar Drift, representative of waters in the Eurasian basin of the Arctic Ocean, and inflowing low-CDOM Atlantic water, where mainly phytoplankton affects the IOPs [*Pavlov et al*., 2015]. Since the sea ice in the region has become significantly thinner and likely younger [*Hansen et al*., 2013], we can examine how melting of a younger Arctic ice pack affects the optical properties of surface waters in these optically diverse waters.

2. Material and Methods

2.1. Sampling and Measurements

Observations were conducted in late summer 2014 in the northern Fram Strait, first during the AREX2014 expedition onboard R/V Oceania (15–22 July 2014) when observations were carried out along sections radiating from the Spitsbergen shelf toward the ice edge to the west and north, and during the FS2014 expedition (24 August 2014 to 4 September 2014) onboard R/V Lance along a section across the Fram Strait at about 79°N (Figure 1), across the West Spitsbergen Current (WSC) and East Greenland Current (EGC) onto the east Greenland shelf [cf. *Granskog et al*., 2012; *Pavlov et al*., 2015].

At all stations, optical properties were measured in situ with an instrument package consisting of an ac-9*plus* attenuation and absorption meter (WET Labs Inc., USA), a Wetstar CDOM fluorometer (WET Labs Inc., USA), a MicroFlu-Chl chlorophyll fluorometer (TrioS GmbH, Germany), and a Seabird SBE 49 FastCAT Conductivity-Temperature-Depth probe (Seabird Electronics, USA). The data stream from all the instruments was merged with DH4 sensor interface module (WET Labs Inc.) and transferred in real time to the deck unit and PC. The ac-9*plus* and CTD water intakes were installed on the same horizontal plane. After passing ac-9*plus*, water was directed with opaque tubing to the flow through cells of both fluorometers. Data were recorded with a frequency of 6 Hz and averaged over 10 records ($\sim$1.6 s). The package was lowered with vertical speed about 0.3 m s^{-1}, giving $\sim$30 cm vertical resolution. The data from instruments were

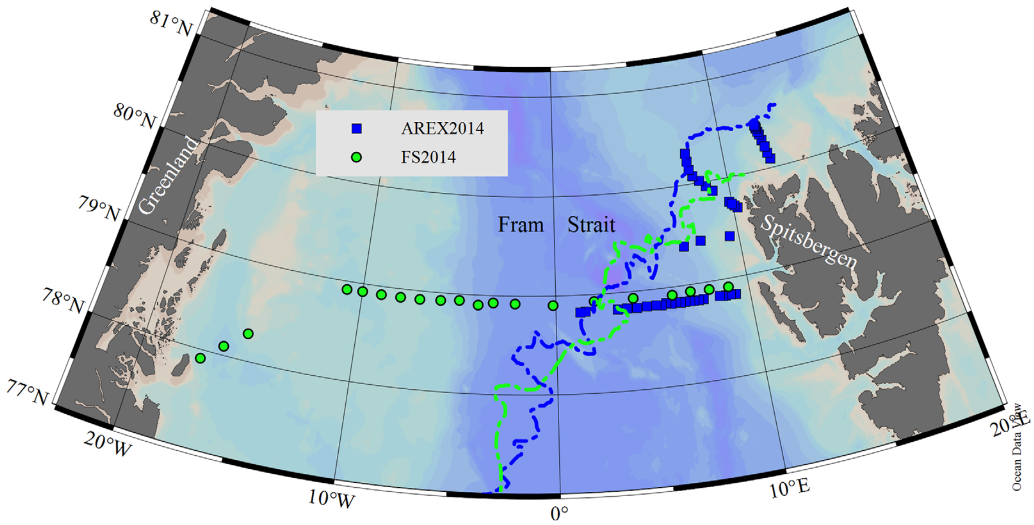

Figure 1. Map of stations during AREX2014 (blue squares) and FS2014 (green circles). Location of approximate ice edge (10% ice concentration), extracted from MET.no ice charts, during the expeditions are indicated with dashed lines of corresponding colors. Produced with Ocean Data View (Schlitzer, R., Ocean Data View, odv.awi.de, 2015).

synchronized using time stamps with Wetlabs Archive Processing (version 4.25) software. A time lag was applied according to positioning of instruments along the tubing and measured flow rates.

In short, the ac-9*plus* measures the absorption and beam attenuation coefficients at nine wavelengths (412, 440, 488, 510, 532, 555, 650, 676, and 715 nm). Temperature and salinity corrections were applied to the signal [*Sullivan et al*., 2006], as well as air and pure water offsets. Values of scattering and absorption by pure water, according to *Pope and Fry* [1997] and *Sogandares and Fry* [1997], were added to determine total absorption (*a*) and total attenuation (*c*) coefficients. Due to use of reflecting tube for the measurement of absorption with ac-9*plus*, the signal requires correction for scattering, which assumes zero absorption at 715 nm [*Zaneveld et al*., 1994]. The instrument was routinely calibrated in ultrapure water and checked for stability with air readings. Scattering (*b*) was determined by subtraction of absorption from attenuation.

The MicroFlu-Chl chlorophyll fluorometer's excitation channel is centered at 470 nm, and the maximum emission light detector is set to 685 nm for chlorophyll a fluorescence and is here reported with 0–5 V DC analog output values for reference. The WetStar CDOM fluorometer was equipped with (custom) excitation at 280 nm and emission at 450 nm, corresponding to the humic-like peak A after *Coble* [1996], and values are presented as raw digital counts with dark offset correction.

All optical elements of the sensors were routinely cleaned every 3–6 casts. During the deployment period, readings from instruments were monitored for fouling; no anomalous readings (as absorption drift) were observed.

2.2. Modeling

The underwater light field was modeled using Ecolight [*Mobley*, 1994]. Calculations were made for the range 350–700 nm with 10 nm increments to facilitate direct comparison with *Pegau* [2002]. Values of absorption and attenuation were extrapolated to 350 nm. In the EGC, an exponential fit between 412 and 510 nm was used (considering CDOM absorption increase with shorter wavelengths [*Granskog et al*., 2012]), while in the CDOM-poor particle-rich WSC waters a linear fit was used. Particle backscatter fraction (b_{bp}/b_p) was chosen to be 0.015 following *Bélanger et al*. [2013]. Bioluminescence and inelastic scatter were not included. Wind speed was set to 4 m s^{-1}. Refraction index of the water was set constant at 1.34. A built-in semiempirical sky model (Radtran) was used with specified solar zenith angle of 65°, representative of noon incident radiation in mid-August in Fram Strait assuming clear sky. The 350–412 nm range contributes <10% of the incident energy in the 350–700 nm range, and exclusion of this part of the spectrum does not change the main conclusions of this work. Calculations were made for the depth range from 1 to 10 m with 1 m vertical step.

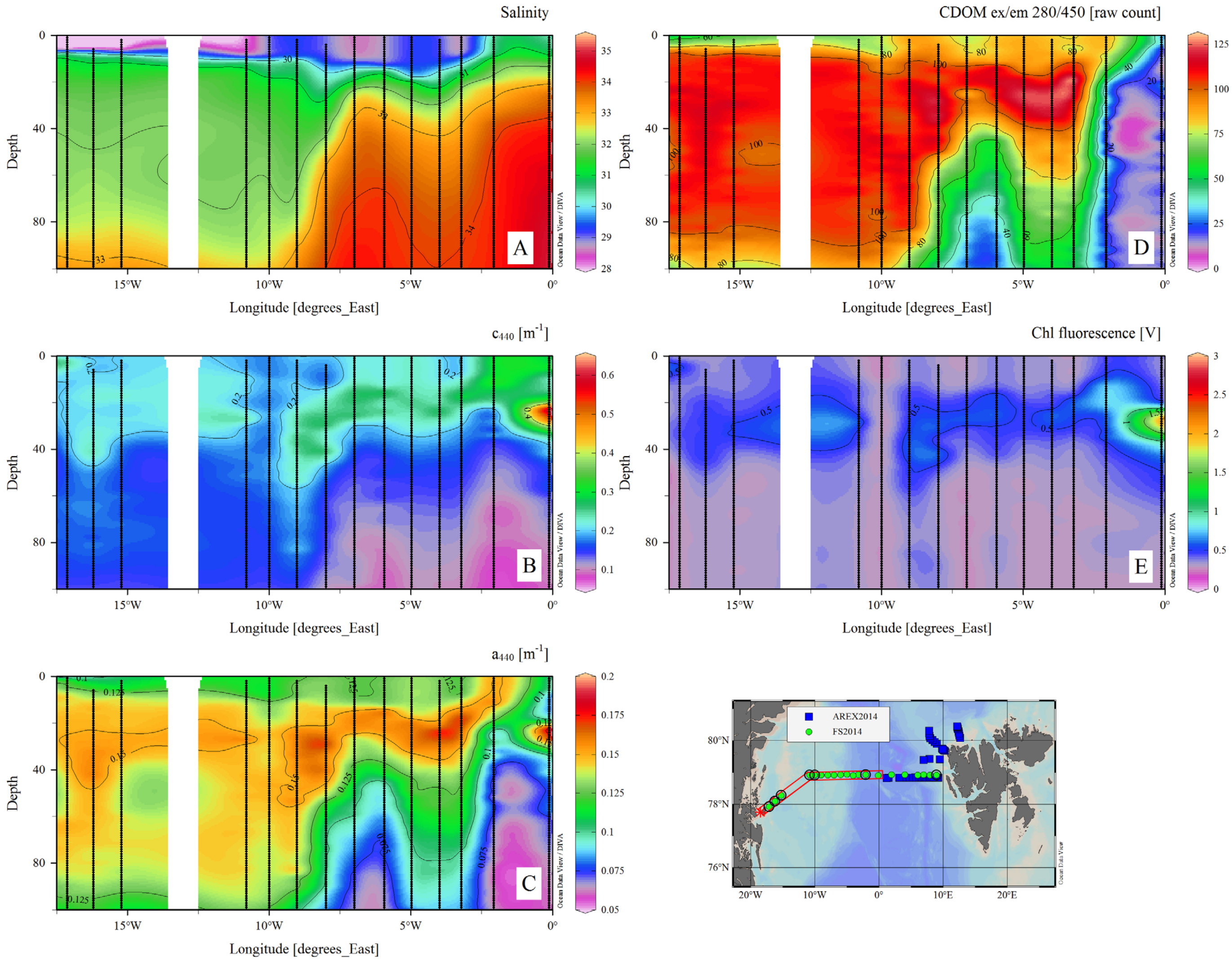

Figure 2. Section across western Fram Strait on east Greenland shelf and in the EGC (see map insert) during FS2014 with: (a) salinity, (b) total attenuation at 440 nm, (c) total absorption at 440 nm, (d) humic-like CDOM fluorescence, and (e) Chl-a fluorescence in the upper 100 m. Produced with Ocean Data View (Schlitzer, R., Ocean Data View, odv.awi.de, 2015).

Underwater profiles of spectral scalar irradiance (E_o, W m^{-2}) were integrated in the range 350 and 700 nm and were used to estimate relative energy deposition between different cases in the upper 10 m layer.

3. Results and Discussion

3.1. Hydrography and IOPs

A typical feature after summer sea-ice melt near the ice edge (AREX2014) and on the partially ice-covered western side of Fram Strait (FS2014) was surface freshening by melting sea ice. At this time of year, a layer of about 10 m thick was significantly fresher than the subsurface waters and thus stratified (Figures 2a and 3a). In this surface layer, a distinct decrease in absorption at shorter wavelengths was evident over CDOM-rich PW on the east Greenland shelf in the EGC, where a humic-like CDOM-rich and near-freezing layer at salinity 32–33 occupied a subsurface layer from about 15 to 90 m depth (Figures 2a and 5a, shown later) [cf. *Granskog et al.*, 2012; *Pavlov et al.*, 2015], representative of the winter mixed layer and originated as halocline waters likely from the Transpolar Drift [*Stedmon et al.*, 2015]. Melting of sea ice into these waters dilutes CDOM concentrations relative to ambient PW (Figures 2d and 5d, shown later) and thus decreases CDOM absorption in the surface layer, because sea-ice melt-derived water contains less CDOM than the ambient subsurface waters. In contrast, the beam attenuation did not change noticeably (Figure 2b; Figure

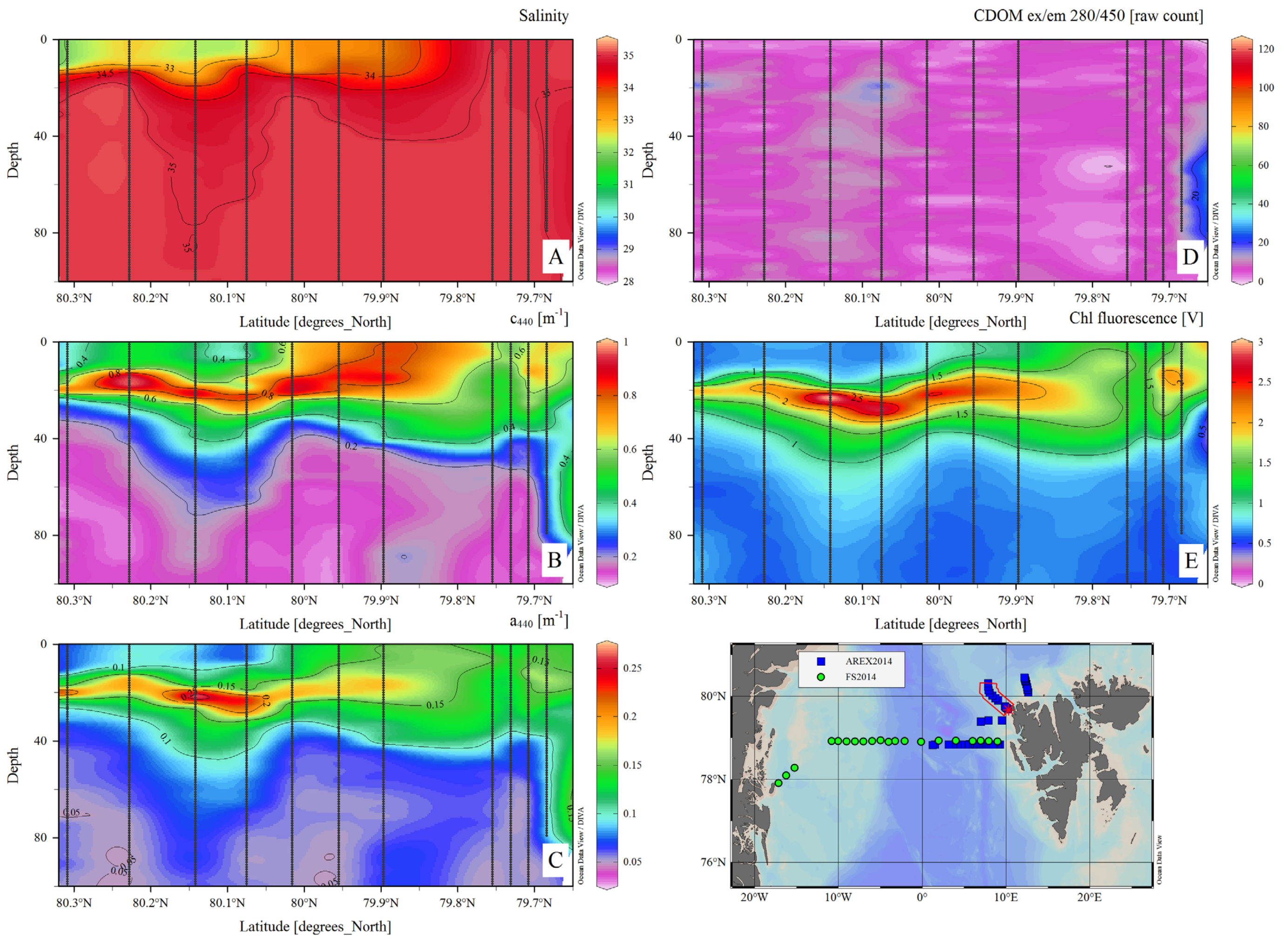

Figure 3. Section from northwestern Spitsbergen shelf to the ice edge across the WSC (see map insert) during AREX2014 with: (a) salinity, (b) total light attenuation at 440 nm, (c) total light absorption at 440 nm, (d) humic-like CDOM fluorescence, and (e) Chl-a fluorescence in the upper 100 m. Produced with Ocean Data View (Schlitzer, R., Ocean Data View, odv.awi.de, 2015).

5b, shown later), which means that scattering increased in this layer, nearly compensating for the decrease in absorption. Since there is no evidence for increased phytoplankton biomass in the surface layer (Figure 2e; Figure 5e, shown later), this material is likely associated with sea-ice melt. This agrees with the findings of *Bélanger et al*. [2013] on increased scattering in underice meltwater layers below multiyear ice. Although the stations nearby Greenland coast could be affected by continental runoff, the stations on the central shelf (around 10 W), far away from runoff sources [*Stedmon et al*., 2015], showed the same exact features with lowered absorption and increased scattering.

Further east on the Fram Strait section and during AREX2014, sea ice melted into more saline and at times warmer Atlantic waters (AW), with very low humic-like CDOM (Figure 3d; Figure 5d, shown later). In these waters, it is apparent that absorption and attenuation are governed by particulate absorption and scattering (Figures 3b–3d), as observed by *Pavlov et al*. [2015], and thus largely controlled by phytoplankton. Thus, the seasonality of light absorption and attenuation is likely high as it depends largely on the seasonality of phytoplankton biomass [cf. *Pavlov et al*., 2015]. Sea-ice melt introduces a fresher and more transparent layer, at least in late summer, with lower absorption and attenuation relative to those of a rather well-mixed surface layer with high chlorophyll in AW closer to the Spitsbergen shelf (Figures 3b and 3c; Figure 5c, shown later). It is likely that sea-ice meltwater is devoid of nutrients, relative to Atlantic water, and does not support excessive phytoplankton growth later in the season [see *Tovar-Sánchez et al*., 2010]. Further, the stratification produced by ice melt may contribute to exhaustion of nutrients in the surface layer and lack of biomass

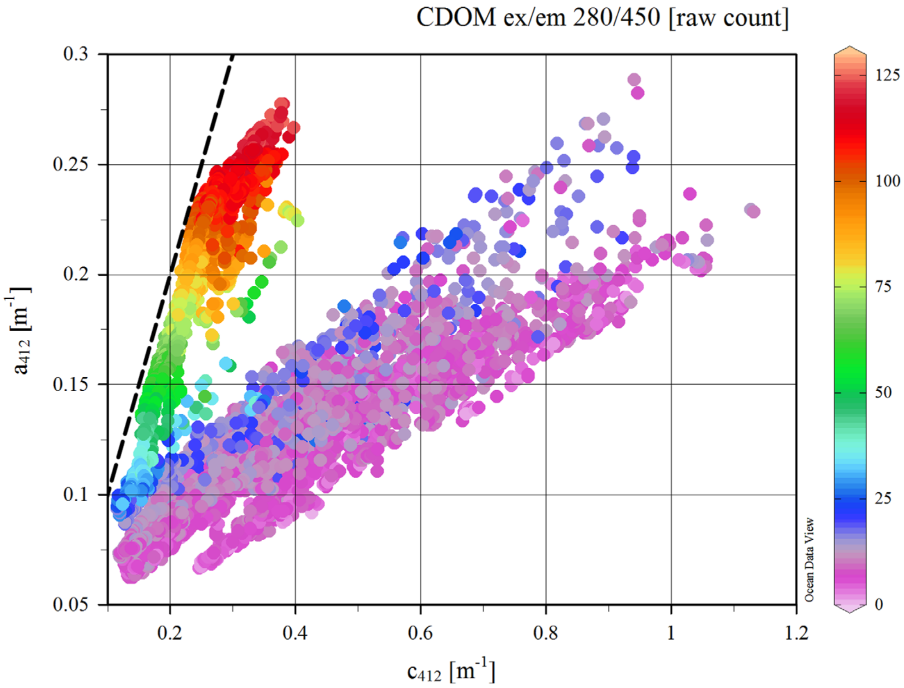

Figure 4. Total light absorption (a_{412}) against total light attenuation (c_{412}) at 412 nm colored with humic-like CDOM fluorescence. The dashed line (1:1 line) indicates when total absorption equals total attenuation. Produced with Ocean Data View (Schlitzer, R., Ocean Data View, odv.awi.de, 2015).

at time of observation. Thus, at least in late summer, subsurface chlorophyll maxima develop near the pycnocline (Figure 3e), which separates the low-salinity nutrient-poor surface layer from the nutrient-rich AW below. In this high-chlorophyll layer below the pycnocline, both absorption and attenuation are high (Figures 3b and 3c).

The contrasting optical properties of the waters in the region are exemplified in Figure 4, where total light absorption is plotted against total light attenuation at 412 nm. In CDOM-rich PW, absorption nearly equals attenuation at shorter wavelengths, thus light attenuation is largely controlled by absorption alone. In the case of PW, CDOM fluorescence (humic like) is strongly correlated with total light absorption at 412 nm (also at 440, 488, and 510 nm; not shown), suggesting the dominance of CDOM absorption for attenuation of light, especially at shorter wavelengths. In the low-CDOM AW, attenuation is largely controlled by other factors, likely absorption and scattering caused by phytoplankton [*Pavlov et al.*, 2015].

3.2. Characteristics of Scattering in Surface Meltwater Layer

We made a qualitative examination of the shape of individual normalized scattering spectra, which could give some indication, but not conclusive evidence, of the type of material in the surface meltwater layer [cf. *Babin et al.*, 2003]. Surface meltwater layer had a tendency for flatter scattering spectra (especially at wavelengths $<$555 nm), similar to Case 2 waters in *Babin et al.* [2003], compared to ambient waters (not shown). This is indicative of phytoplankton-derived particles coexisting with minerals in suspension [*Babin et al.*, 2003]. Nevertheless, this does not give conclusive evidence on the type of scattering material associated with ice melt, as it could also be affected, for example, by changes in particle absorption (thus composition) and size distribution of the particles themselves [*Babin et al.*, 2003; *Doxaran et al.*, 2009]. The particulate matter composition, especially the origin of scattering particles, in sea-ice meltwaters thus merits further study.

3.3. Typical Profiles

Figure 5 summarizes the three main types of absorption and attenuation profiles encountered in the region; (i) melting of sea ice into CDOM-rich PW in the EGC on the east Greenland shelf, (ii) sea-ice meltwater layer in AW at the ice edge in the WSC, and (iii) in the absence of ice melt, a rather well-mixed AW near the Spitsbergen shelf near the core of the WSC. In the Atlantic-dominated waters, absorption is not related to

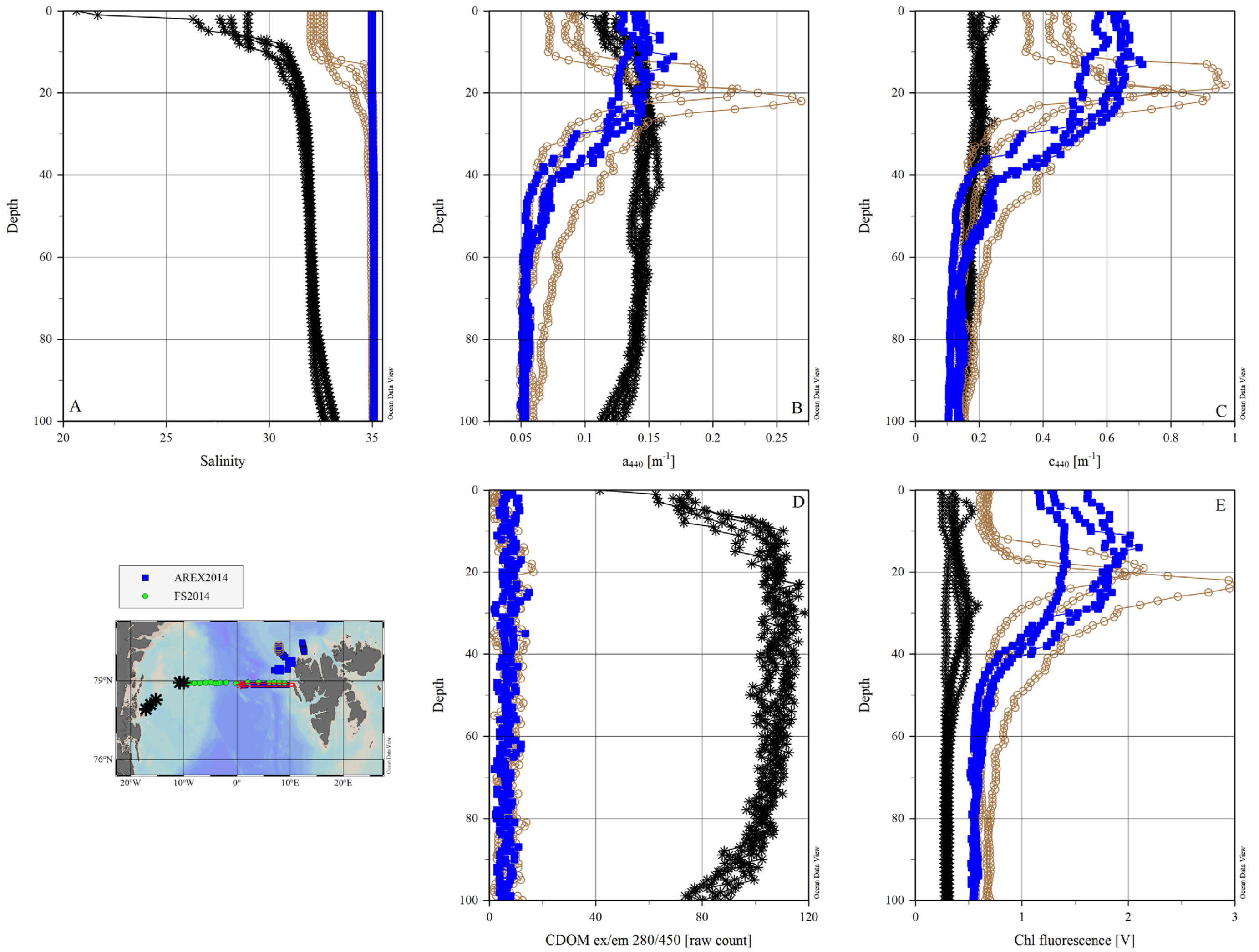

Figure 5. Typical profiles of (a) salinity, (b) total absorption at 440 nm, (c) beam attenuation at 440 nm, (d) humic-like CDOM fluorescence, and (e) chlorophyll fluorescence. Black stars, brown open circles, and blue squares symbols denote stations on east Greenland shelf (FS2014), at ice edge with meltwater layer (AREX2014), and in well-mixed Atlantic waters (AREX2014), respectively. Produced with Ocean Data View (Schlitzer, R., Ocean Data View, odv.awi.de, 2015).

humic-like CDOM but rather to chlorophyll fluorescence and thus phytoplankton biomass (see also Figure 3). This supports the findings of *Pavlov et al.* [2015] from water samples of dissolved and particulate absorption across Fram Strait roughly at the same time of the year.

As noted above, in EGC surface waters influenced by ice melt, the attenuation is basically unaffected (Figure 5c), and thus increased scattering in this layer compensates for lowered absorption (Figure 5b). In WSC waters, the ice melt layer clearly lowers both absorption and attenuation (Figures 5b and 5c), both relative to the subsurface chlorophyll maxima and the well-mixed WSC waters closer to Spitsbergen. In the absence of CDOM (Figure 5d), it is likely due to less phytoplankton growth or particulates in general in the ice melt layer compared to the higher biomass waters in the core of the WSC and in the subsurface layer (Figure 5e).

3.4. Comparison to Earlier Observations in High Arctic

Comparing the observed values of total absorption and attenuation in the EGC to those presented by *Pegau* [2002] from the western Arctic, some distinct differences can be found (Table 1). In the absence of algal biomass, both EGC cases (with and without sea-ice melt) show considerably higher absorption and attenuation, especially at shorter wavelengths, than the "clear water" case, without phytoplankton, observed by *Pegau* [2002] (hereafter PC). Absorption at shorter wavelengths is significantly higher in EGC subsurface waters than those reported by *Pegau* [2002]. EGC subsurface waters represent the ambient water mass the ice has

Table 1. Tabulated Values of Typical Total Light Absorption (*a*) and Total Light Attenuation (*c*) for This Study[a]

	EGC With Sea-Ice Melt		EGC Subsurface Waters		WSC With Sea-Ice Melt		WSC Well-Mixed Surface Layer		*Pegau* [2002] Turbid Case (PT)		*Pegau* [2002] Clear Case (PC)		Clearest Natural Waters [*Smith and Baker*, 1981] (CN)	
Wavelength	*a*	*c*	*a*	*c*	*a*	*c*	*a*	*c*	*a*	*c*	*a*	*c*	*a*	*c*
350[b]	0.522	0.602	0.713	0.758	0.146	0.480	0.240	0.710	n/a	n/a	n/a	n/a	0.046	0.060
412	0.192	0.273	0.242	0.299	0.106	0.453	0.159	0.654	0.155	0.320	0.121	0.159	0.016	0.023
440	0.123	0.199	0.149	0.201	0.085	0.423	0.141	0.618	0.117	0.278	0.085	0.125	0.014	0.019
488	0.076	0.149	0.085	0.137	0.064	0.399	0.106	0.585	0.079	0.237	0.052	0.091	0.019	0.022
510	0.077	0.149	0.084	0.135	0.069	0.402	0.097	0.589	0.078	0.236	0.059	0.095	0.036	0.038
532	0.079	0.149	0.084	0.134	0.071	0.404	0.095	0.589	0.078	0.233	0.063	0.102	0.050	0.053
555	0.086	0.152	0.090	0.137	0.080	0.406	0.092	0.589	0.084	0.236	0.076	0.113	0.067	0.069
650	0.352	0.407	0.352	0.391	0.351	0.648	0.359	0.821	0.349	0.480	0.342	0.375	0.349	0.350
676	0.462	0.506	0.463	0.490	0.468	0.746	0.490	0.920	0.472	0.595	0.458	0.489	0.440	0.441

[a]EGC with sea-ice melt—average *a* and *c* for six stations in the EGC for the 0–10 m layer; EGC subsurface waters—average a and c for the layer 20–50 m (representative of the winter mixed layer before ice melt) for same six stations; WSC with sea-ice melt—average *a* and *c* values for the layer 0–10 m for three sea-ice melt influenced stations at the ice edge; WSC well-mixed surface layer—average *a* and *c* for three stations without ice melt influence. For comparison, two cases (turbid and clear) of *Pegau* [2002] in western Arctic and those of clearest natural waters (CN) from *Smith and Baker* [1981] are shown.

[b]Values at 350 nm have been extrapolated from the observed data (see text).

melted into, i.e., the likely conditions during the end of winter in the mixed layer. With dilution by sea-ice melt in the EGC, absorption is higher at shorter wavelengths than for the "turbid" case (caused by a phytoplankton bloom) reported by *Pegau* [2002] (hereafter PT). The presence of phytoplankton in PT increased scattering compared to the low-chl-a waters in the EGC, so that the total light attenuation in the EGC subsurface waters is quite similar to that in PT (Table 1). This indicates that the optical properties in the Eurasian basin are quite different to those reported from the western Arctic, due to the significant load of terrigenous CDOM through Siberian rivers, transported with the Transpolar Drift [*Stedmon et al*., 2011, 2015; *Granskog et al*., 2012]. Thus, especially for the Eurasian basin, the description of light attenuation in models needs to be revisited, and a physically based parameterizations could be based on the influence of riverine waters (in essence CDOM) in addition to seasonality of phytoplankton.

In WSC waters influenced by sea-ice melt, absorption is quite similar to the clear case (PC) by *Pegau* [2002] (Table 1), while the contribution from scattering is higher. In the well-mixed WSC case, both absorption and attenuation are significantly higher than in the PC case (Table 1). Compared to the PT case linked to high phytoplankton biomass, the absorption in well-mixed WSC waters is similar, but the attenuation (and thus scattering) significantly higher than for PT (Table 1). This could be due to the intensity of the phytoplankton blooms in the region adjacent to Spitsbergen, which is ice free most of the summer.

3.5. Effect of Sea-Ice Meltwaters on Light Climate

To examine the effect of the sea-ice meltwaters on light climate and radiative heating in the EGC and WSC, we use the above typical cases (Table 1) as input to the Ecolight model [*Mobley*, 1994], with focus on the effect in the upper 10 m, as this is the layer that is influenced by ice melt (Figures 2, 3, and 5). We assume a homogeneous layer from surface to 10 m depth [cf. *Pegau*, 2002], as in many cases that was a fair approximation, and we examine how the optical properties of surface waters with sea-ice melt compare to those with no ice melt in the EGC and WSC, and to the cases presented by *Pegau* [2002] from the western Arctic, and to the clearest natural waters [*Smith and Baker*, 1981]. The results are summarized in Figure 6 and Table 2.

Profiles of scalar irradiance in the range 350–700 (E_o), normalized to incoming incident scalar irradiance just below the sea surface (E_o (0-)), show strongest attenuation in the upper 0–2 m, driven by pure water absorption (Figure 6a). In clearest natural waters (CN), light attenuation is by far the lowest compared to other cases with more than 40% of E_o relative to E_o (0-) reaching 10 m. Generally, stronger attenuation is found in two EGC cases with 10–15% of E_o available at 10 m. For both WSC and PT cases, E_o values at 10 m range between 15 and 20%. PC is a case with lowest attenuation among all cases from the Arctic Ocean with E_o of 23% at 10 m.

The sea-ice meltwater layer results in less heat absorption in the upper 3–5 m compared to the ambient cases in both EGC and WSC in late summer (solid lines; Figure 6b). This is especially significant in the case for WSC where the ambient conditions with high chl throughout the mixed layer (Figure 5) are replaced

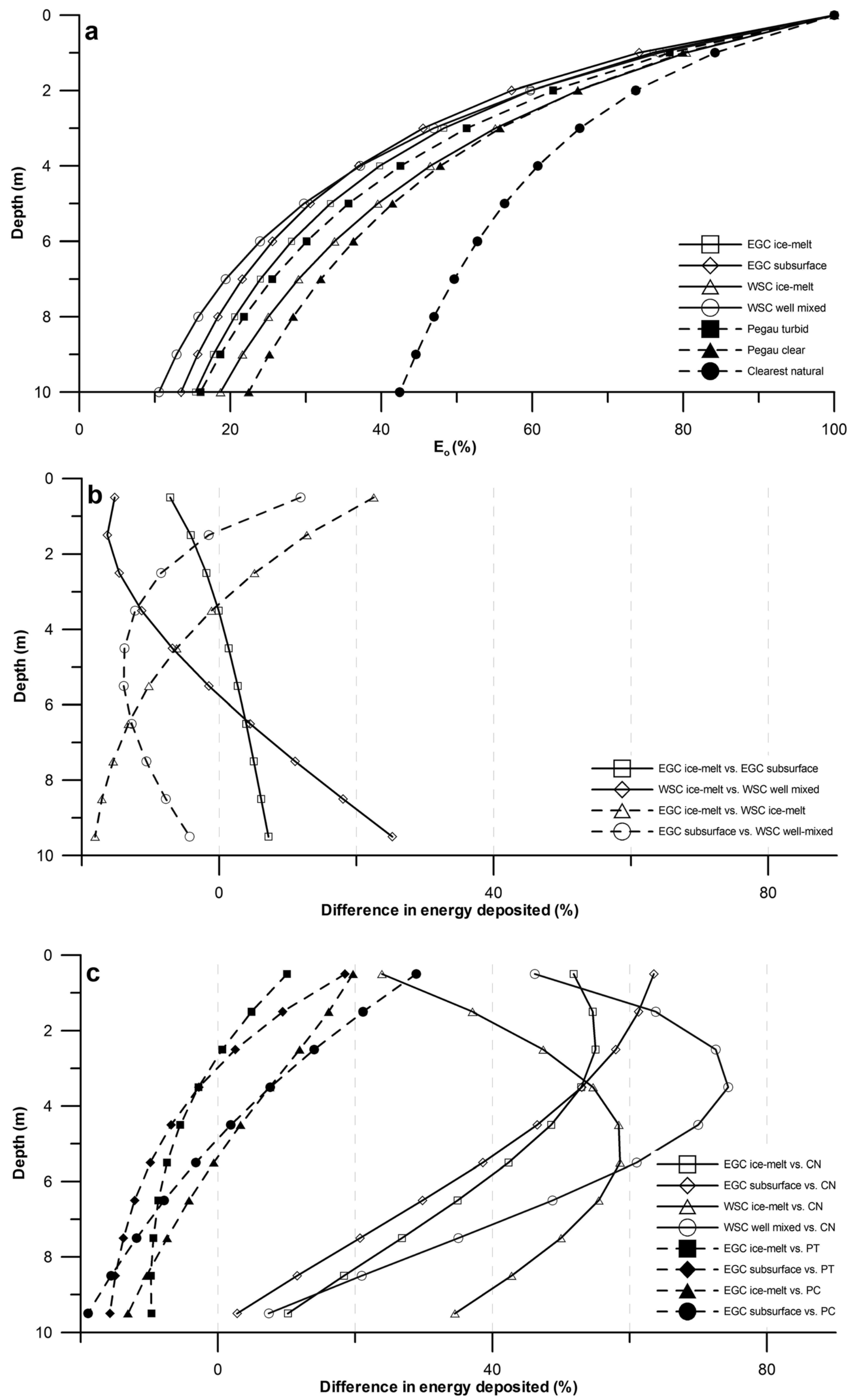

Figure 6. (a) Modeled scalar irradiance E_o(350–700) relative to E_o(0-) for the typical cases (Table 1). And comparison of energy deposited (b) relative to no meltwater layer cases and (c) relative to clearest natural waters (CN) and the turbid (PT) and clear (PC) cases from *Pegau* [2002]. For details see text.

with a significantly more transparent surface sea-ice meltwater layer, which results in about 15% less heat deposited in the top 2 m (9% in the top 10 m, Table 2). The corresponding figures for the EGC waters are about 6% and 2%, respectively. Thus, there is a modest change due to the changes in transparency in the

Table 2. Difference in Energy Absorbed (%) in Different Depth Ranges Between Cases Considered in This Study

Depth Range (m)	EGC Ice Melt Versus Subsurf	WSC Ice Melt Versus Well Mixed	EGC Ice Melt Versus WSC Ice Melt	EGC Subsurf Versus WSC Well Mixed	EGC Ice Melt Versus CN	EGC Subsurface Versus CN
0–1	−7.1	−15.2	22.5	11.9	51.8	63.5
0–2	−6.0	−15.7	18.4	6.2	52.9	62.6
0–5	−3.9	−13.9	10.4	−1.2	52.9	59.0
0–10	−2.2	−9.1	4.1	−3.3	47.0	50.3
Depth Range (m)	**WSC Ice Melt Versus CN**	**WSC Well Mixed Versus CN**	**EGC Ice Melt Versus PT**	**EGC Subsurface Versus PT**	**EGC Ice Melt Versus PC**	**EGC Subsurface Versus PC**
0–1	23.9	46.2	10.1	18.5	19.7	28.9
0–2	29.2	53.2	7.9	14.7	18.2	25.7
0–5	38.5	60.9	3.7	7.9	14.1	18.6
0–10	41.2	55.4	0.8	3.1	9.1	11.5

CDOM-rich EGC while the effect becomes quite significant when meltwater results in a chl-poor layer in the WSC.

In EGC waters, where CDOM dominates absorption and attenuation (Figure 4) and phytoplankton biomass is low, the upper 2 m accumulate 18% and 26% more heat than for PC in western Arctic (Figure 6c and Table 2). The corresponding values for the upper 10 m are 9% and 12%, respectively. This reveals the influence of the high-CDOM levels in the Arctic outflow in Fram Strait [cf. *Granskog et al.*, 2012; *Pavlov et al.*, 2015] in the absence of phytoplankton blooms. Also relative to the PT case, the upper 2 m in the EGC accumulate about 8% and 15% more heat than for the ice-melt and ambient case, respectively. In the course of summer, this is a significant addition of heat at the very surface, which could accelerate ice melt in CDOM-rich waters in the Eurasian basin.

Relative to the clearest natural waters (CN) [*Smith and Baker*, 1981], 50–60% more heat accumulates in upper meters in the EGC (for both the ambient and ice melt cases) (Table 2), significantly higher than what has been reported from western Arctic [*Pegau*, 2002; *Hill*, 2008]. In the WSC, the corresponding numbers are 40% for the ice-melt case, and 55% in the ambient case for the upper 10 m (Figure 6c and Table 2); however, in the latter case, these are likely controlled by transient phytoplankton blooms, while the high-CDOM conditions are likely to prevail year round for waters in the Transpolar Drift.

4. Conclusions

We have observed the inherent optical properties of surface waters affected by sea-ice melt in late summer across water masses spanning from high-CDOM Polar Water to low-CDOM Atlantic waters in the northern Fram Strait. In both cases, less heat is deposited in the upper meters in late summer, than in absence of surface freshening by ice melt (Table 2 and Figure 6c).

In Polar Water, likely representative of conditions for the surface waters of much of the Eurasian basin and Transpolar Drift in particular, CDOM governs absorption and attenuation, and results in higher radiative heating in the upper meters compared to the western Arctic [cf. *Pegau*, 2002], even when diluted by sea-ice melt. This may have some bearing on the sea-ice melt rates over different water masses. Sea-ice melt dilutes CDOM concentrations in Polar Water, and sea ice is an unlikely source of excess CDOM during melt over Polar surface waters. Thus, the absorption of CDOM decreases, but is apparently compensated by increased scattering, that results in little change in total attenuation, however, this likely depends on the type of ice that melts. The origin of increased scattering in ice melt waters remains unknown, but is in agreement with the findings of *Bélanger et al*. [2013] in the western Arctic from melting multiyear ice. This warrants further study, as it could be specific to the processes occurring in sea ice during its formation or melt, such as release of atmospheric deposition, ice algae, or a combination of these.

In the region dominated by Atlantic water north of Spitsbergen, phytoplankton govern the IOPs [cf. *Pavlov et al*., 2015], and introduction of a sea-ice melt layer significantly decreases absorption and attenuation, at least in late summer when the spring bloom has declined. Neither in low-CDOM AW sea-ice melt appears to be a source of excess CDOM. Increased transparency is likely due to limited phytoplankton growth in the surface layer above the pycnocline, which separates the surface layer from high-nutrient waters of Atlantic origin. Subsurface chlorophyll maxima appear to be ubiquitous in Atlantic waters affected by ice melt in late summer, in part supported by the relatively nutrient-rich waters below the pycnocline, and likely favorable light conditions due to the transparent surface layer.

In summary, we have shown that in the surface waters of the Transpolar Drift, the high loading of CDOM results in high radiant heating rates in the upper meters relative to the western Arctic, which may have some bearing on the ice melt rates across different Arctic basins. The effect of sea-ice meltwaters on the light attenuation depends on the ambient water masses and likely also the time of year, especially regards phytoplankton blooms. Sea-ice melt is not a noteworthy source of CDOM, as previously speculated [*Scully and Miller*, 2000]. There were indications for higher scattering in sea-ice meltwaters [cf. *Bélanger et al*., 2013], and the reason for this needs to be examined closer. More transparent surface layers increase heat deposition at depth, and in conjunction with stratification induced by meltwaters, accumulated heat is not immediately available for ice melt [cf. *Hudson et al*., 2013]. Correctly describing the effect of sea-ice melt on the light climate, and stratification of the upper ocean, is crucial to be able to correctly assess solar heating and productivity in Arctic surface waters.

Acknowledgments
We thank the crews of R.V. Lance and R.V. Oceania and colleagues for the help onboard. We thank Jennifer King and Max König for help with sea ice edge data. This work was supported by the Polish-Norwegian Research Programme operated by the National Centre for Research and Development under the Norwegian Financial Mechanism 2009–2014 in the frame of Project Contract Pol-Nor/197511/40/2013, CDOM-HEAT. M.A.G. was supported by the Centre for Ice, Climate and Ecosystems (ICE) at the Norwegian Polar Institute. The data used in the paper will be available upon request (e-mail: mats@npolar.no) in compliance with the American Geophysical Union Publications Data Policy. Constructive comments from an anonymous reviewer and Ian Walsh improved the paper.

References

Arrigo, K. R., G. van Dijken, and S. Pabi (2008), Impact of a shrinking Arctic ice cover on marine primary production, *Geophys. Res. Lett.*, *35*, L19603, doi:10.1029/2008GL035028.

Babin, M., A. Morel, V. Fournier-Sicre, F. Fell, and D. Stramski (2003), Light scattering properties of marine particles in coastal and open ocean waters as related to the particle mass concentration, *Limnol. Oceanogr.*, *48*(2), 843–859, doi:10.4319/lo.2003.48.2.0843.

Bélanger, S., H. Xie, N. Krotkov, P. Larouche, W. F. Vincent, and M. Babin (2006), Photomineralization of terrigenous dissolved organic matter in Arctic coastal waters from 1979 to 2003: Interannual variability and implications of climate change, *Global Biogeochem. Cycles*, *20*, GB4005, doi:10.1029/2006GB002708.

Bélanger, S., S. A. Cizmeli, J. Ehn, A. Matsuoka, D. Doxaran, S. Hooker, and M. Babin (2013), Light absorption and partitioning in Arctic Ocean surface waters: Impact of multiyear ice melting, *Biogeosciences*, *10*(10), 6433–6452, doi:10.5194/bg-10-6433-2013.

Coble, P. G. (1996), Characterization of marine and terrestrial DOM in seawater using excitation-emission matrix spectroscopy, *Mar. Chem.*, *51*(4), 325–346.

Doxaran, D., K. Ruddick, D. McKee, B. Gentili, D. Tailliez, M. Chami, and M. Babin (2009), Spectral variations of light scattering by marine particles in coastal waters, from visible to near infrared, *Limnol. Oceanogr. Methods*, *54*(4), 1257–1271, doi:10.4319/lo.2009.54.4.1257.

Granskog, M. A., R. W. Macdonald, C.-J. Mundy, and D. G. Barber (2007), Distribution, characteristics and potential impacts of chromophoric dissolved organic matter (CDOM) in Hudson Strait and Hudson Bay, Canada, *Cont. Shelf Res.*, *27*, 2032–2050, doi:10.1016/j.csr.2007.05.001.

Granskog, M. A., C. A. Stedmon, P. A. Dodd, R. M. W. Amon, A. K. Pavlov, L. de Steur, and E. Hansen (2012), Characteristics of colored dissolved organic matter (CDOM) in the Arctic outflow in the Fram Strait: Assessing the changes and fate of terrigenous CDOM in the Arctic Ocean, *J. Geophys. Res.*, *117*, C12021, doi:10.1029/2012JC008075.

Hansen, E., S. Gerland, M. A. Granskog, O. Pavlova, A. H. H. Renner, J. Haapala, T. B. Løyning, and M. Tschudi (2013), Thinning of Arctic sea ice observed in Fram Strait: 1990-2011, *J. Geophys. Res. Oceans*, *118*, 5202–5221, doi:10.1002/jgrc.20393.

Hill, V. J. (2008), Impacts of chromophoric dissolved organic material on surface ocean heating in the Chukchi Sea, *J. Geophys. Res.*, *113*, C07024, doi:10.1029/2007JC004119.

Hudson, S. R., M. A. Granskog, A. Sundfjord, A. Randelhoff, A. H. H. Renner, and D. V. Divine (2013), Energy budget of first-year Arctic sea ice in advanced stages of melt, *Geophys. Res. Lett.*, *40*, 2679–2683, doi:10.1002/grl.50517.

Kirk, J. T. O. (1994), *Light and Photosynthesis in Aquatic Ecosystems*, Cambridge Univ. Press, Cambridge, U. K.

Meier, W. N., et al. (2014), Arctic sea ice in transformation: A review of recent observed changes and impacts on biology and human activity, *Rev. Geophys.*, *52*, 185–217, doi:10.1002/2013RG000431.

Mobley, C. D. (1994), *Light and Water, Radiative Transfer in Natural Waters*, Academic, San Diego, Calif.

Nicolaus, M., C. Katlein, J. Maslanik, and S. Hendricks (2012), Changes in Arctic sea ice result in increasing light transmittance and absorption, *Geophys. Res. Lett.*, *39*, L24501, doi:10.1029/2012GL053738.

Pavlov, A. K., M. A. Granskog, C. A. Stedmon, B. V. Ivanov, S. R. Hudson, and S. Falk-Petersen (2015), Contrasting optical properties of surface waters across the Fram Strait and its potential biological implications, *J. Mar. Syst.*, *143*, 62–72, doi:10.1016/j.jmarsys.2014.11.001.

Pegau, W. S. (2002), Inherent optical properties of the central Arctic surface waters, *J. Geophys. Res.*, *107*(C10), 8035, doi:10.1029/2000JC000382.

Pope, R., and E. Fry (1997), Absorption spectrum (380-700 nm) of pure water. II. Integrating cavity measurements, *Appl. Opt.*, *36*, 8710–8723, doi:10.1364/AO.36.008710.

Popova, E. E., A. Yool, A. C. Coward, F. Dupont, C. Deal, S. Elliott, E. Hunke, M. Jin, M. Steele, and J. Zhang (2012), What controls primary production in the Arctic Ocean? Results from an intercomparison of five general circulation models with biogeochemistry, *J. Geophys. Res.*, *117*, C00D12, doi:10.1029/2011JC007112.

Scully, N., and M. W. L. Miller (2000), Spatial and temporal dynamics of colored dissolved organic matter in the north water polynya, *Geophys. Res. Lett.*, *27*, 1009–1011.

Smith, R. C., and K. S. Baker (1981), Optical properties of the clearest natural waters (200-800 nm), *Appl. Opt.*, *20*, 177–184, doi:10.1364/AO.20.000177.

Sogandares, F., and E. Fry (1997), Absorption spectrum (340-640 nm) of pure water. I. Photothermal measurements, *Appl. Opt.*, *36*, 8699–8709, doi:10.1364/AO.36.008699.

Stedmon, C. A., R. M. W. Amon, A. J. Rinehart, and S. A. Walker (2011), The supply and characteristics of colored dissolved organic matter (CDOM) in the Arctic Ocean: Pan Arctic trends and differences, *Mar. Chem.*, *124*(1), 108–118.

Stedmon, C. A., M. A. Granskog, and P. A. Dodd (2015), An approach to estimate the freshwater contribution from glacial melt and precipitation in East Greenland shelf waters using colored dissolved organic matter (CDOM), *J. Geophys. Res. Oceans*, *120*, 1107–1117, doi:10.1002/2014JC010501.

Sullivan, J. M., M. S. Twardowski, J. R. V. Zaneveld, C. M. Moore, A. H. Barnard, P. L. Donaghay, and B. Rhoades (2006), The hyperspectral temperature and salt dependencies of absorption by water and heavy water in the 400 - 750 nm spectral range, *Appl. Opt.*, *45*, 5294–5309.

Tovar-Sánchez, A., C. M. Duarte, J. C. Alonso, S. Lacorte, R. Tauler, and C. Galbán-Malagón (2010), Impacts of metals and nutrients released from melting multiyear Arctic sea ice, *J. Geophys. Res.*, *115*, C07003, doi:10.1029/2009JC005685.

Zaneveld, J. R. V., J. C. Kitchen, and C. Moore (1994), The scattering error correction of reflecting-tube absorption meters, *Proc. SPIE Soc. Opt. Eng.*, *2258*, 44–55.